Addressing Grid Nonlinearities in Discrete Electromechanical Oscillation Control

Sebastian Martinez-Lizana, Héctor Pulgar-Painemal
Department of Electrical Engineering and Computer Science
University of Tennessee, Knoxville, TN, 37996
smart118@vols.utk.edu, hpulgar@utk.edu

***Abstract*—This paper progresses on the development of the discrete electromechanical oscillation control (DEOC). The DEOC approach is based on the step-wisely control of electronically-interfaced resources' (EIR) power output and aims to significantly reduce the amplitude of multiple oscillatory modes in power systems. The theoretical formulation of the problem and the proposed solution is described. This work addresses the issues of a nonlinear grid representation and favorable reduction of control actions from EIRs, as well as their impact on the DEOC performance. Simulations on a 9-bus system validate the effectiveness of the proposed control even when highly load scenarios are considered.**

***Index Terms*—inter-area oscillations, oscillation damping, discrete control, power system control, power system oscillations.**

I. Introduction

At this moment, the amount of renewable power integrated into electrical power systems only covers a small part of the total load. The rest of the load is for the largest part covered by conventional thermal, nuclear, and hydropower plants. As long as the renewable penetration level is low, the overall dynamic behavior of the power system is expected to be determined by synchronous generators. However, in some network areas, wind turbines and PV solar plants have been gradually starting to replace the output of conventional generators, especially during periods with low load and much wind [1]–[3].

This situation leads to a soaring risk of more recurrent appearances of poorly damped oscillations. Inertia distribution and grid topology have been detected as relevant factors involved with the appearance of critical oscillations [4], [5]. This situation can be aggravated if renewable resources are deployed away from load centers, thus increasing stress on the transmission system [6]. Consequently, oscillations can become a critical problem in the forthcoming grid.

The design of new control systems and the expansion of the grid control capabilities may pose a suitable solution to overcome these approaching problems [7], [8]. As well as with continuous control, multiple attempts to handle oscillations have been proposed with discrete controllers. The main idea behind these proposals is the use of elements with fast switching capabilities such as series-connected switching capacitors, SVC, or STATCOMs to return to the system equilibrium point in minimum time after a disturbance [9]–[11]. Although several of these approaches have proven to be effective for simplified systems, practical issues such as model aggregation, lack of multi-mode representation [12], [13], and fault location dependency make these work burdensome to real applications.

A new approach to discrete control has been proposed in [14] and [15]. The so-called discrete electromechanical oscillation control (DEOC) aims to enable emerging power technologies for oscillation control. Wind power and PV solar plants are exploited by enabling a discrete control logic to transiently reduce their power output without the need for curtailment. Moreover, battery energy storage systems can be controlled for both injection or absorption of power in a discrete fashion. This is possible due to their inverter-based coupling to the power grid, which can be controlled quickly compared to transient stability-related power system dynamics.

Previous research works that deal specifically with the DEOC problem have proposed the fundamental concepts behind this control strategy. In order to do so, assumptions have been made to develop a closed-form solution that can effectively provide a procedure to determine the required power injection/absorption by controllable components (CCs), and synthesis of switching functions [14], [15]. This paper dispenses some of these assumptions by:

- considering a nonlinear representation of the grid by means of the classical power flow formulation, and
- reducing the number of required CCs by working only with buses with high mode controllability with respect to the electromechanical modes of interest.

Simulations in the IEEE 9-bus system verify the findings of this work. This paper is structured as follows. Section II describes the theoretical development of the DEOC including models used, overall DEOC operation, discrete power injection by CCs, and switching conditions. Section III presents simulation results and control performance. Finally, conclusions are presented in Section IV.

II. Discrete Electromechanical Oscillation Control (DEOC)

DEOC aims to enable discrete control mechanisms that inject/absorb active power at a given set of buses. This set corresponds to buses whose connected elements (EIRs) can step-wisely adjust their power output, such as energy storage systems, PV solar generation, and wind turbines. This section

This material is based upon work supported by the National Science Foundation under NSF CAREER Grant No. 2044629. This work also made use of shared facilities supported by the Engineering Research Center Program of the National Science Foundation and the Department of Energy under NSF Award No. EEC-1041877 and the CURENT Industry Partnership Program.

2023 North American Power Symposium (NAPS) | 979-8-3503-1509-7/23/$31.00 ©2023 IEEE | DOI: 10.1109/NAPS58826.2023.10318657

discusses the DEOC foundations for a general formulation based on a nonlinear grid representation.

A. Models

1) Synchronous generators: consider the generator i represented with a classical model neglecting the damping

$$\frac{d\delta_i}{dt} = \omega_s\left(\omega_i - 1\right) \tag{1}$$

$$\frac{d\omega_i}{dt} = \frac{1}{2H_i}\left(P_{mi} - P_{ei}\right) \tag{2}$$

where δ_i is the torque angle in radians, ω_s is the synchronous speed (377 rad/s for a 60 Hz system), ω_i is the speed deviation in per unit, H_i is the inertia constant in seconds, P_{mi} is the mechanical power input in per unit, and P_{ei} is the electrical power output of generator i in per unit. The electrical power is derived from the machine equivalent circuit of Fig. 1 as

$$P_{ei} = \mathrm{Re}\left\{E_i e^{j\delta_i}\bar{I}_i^*\right\} = E_i i_{xi}\cos\delta_i + E_i i_{yi}\sin\delta_i \tag{3}$$

In addition, from the same circuit, the algebraic equation that connects the machine to the grid is

$$E_i e^{j\delta_i} = \left(i_{xi} + j i_{yi}\right) j X_{di}^{'} + V_i e^{j\theta_i} \tag{4}$$

when separated into real and imaginary parts leads to

$$V_i\cos\theta_i = E_i\cos\delta_i + X_{di}^{'} i_{yi} \tag{5}$$

$$V_i\sin\theta_i = E_i\sin\delta_i - X_{di}^{'} i_{xi} \tag{6}$$

with i_{di} and i_{qi} the SG i corresponding algebraic variables.

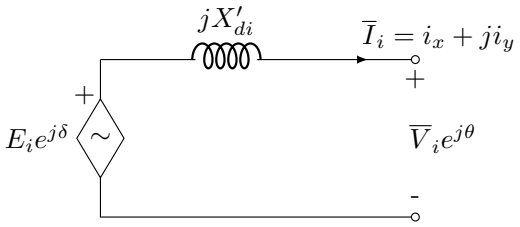

Fig. 1. SG classical model equivalent circuit.

2) Grid: consider the admittance matrix formulation to represent the n_b-buses power grid as follows

$$\bar{I}_b = Y_{bus}\bar{V}_b \tag{7}$$

where the current and voltage injection vectors are defined as $\bar{I}_b = [\bar{I}_1 \quad \bar{I}_2 \quad \cdots \bar{I}_n]^T$, and $\bar{V}_b = [\bar{V}_1 \quad \bar{V}_2 \quad \cdots \bar{V}_n]^T$, with $\bar{V}_i = V_i e^{j\theta_i}$. When separated into real and imaginary parts, result in $2n_b$ algebraic equations to represent the grid.

The current injection $\bar{I}_i$ at PQ and PV buses is given by

$$\bar{I}_i = \frac{\bar{S}_i^*}{\bar{V}_i^*} = \frac{P_i - jQ_i}{V_i}e^{j\theta_i} \tag{8}$$

$$\bar{I}_i = i_{xi} + j i_{yi} \tag{9}$$

respectively. With $\bar{S}_i = P_i + jQ_i$ being the complex power consumption at the PQ bus. For PV buses, the current components i_{xi}, and i_{yi} are the algebraic variables of the corresponding synchronous generator.

3) Controllable components: given that EIRs are assumed to be step-wisely controlled, consider m CCs with their active power output given by

$$P_{ref} = P_{ref}^0 + \Delta P\left(\mu_{t_{on}} - \mu_{t_{off}}\right) \tag{10}$$

with $P_{ref}, P_{ref}^0, \Delta P \in \mathbb{R}^m$. P_{ref}^0 is the initial power set-point vector, ΔP is a vector that contains a predefined quantity for every CC, and must be determined based on both the particular characteristic of the system under study and the number of CCs, $\mu_\tau = 1, \forall t > \tau$ is the unit step function, and t_{on}, and t_{off} the switching times with $t_{off} > t_{on}$.

B. DEOC operation

A n_b-buses power system with $n_g - 1$ SGs represented by a classical model and one slack bus, m controllable components, and the admittance formulation for the grid can be represented by the following set of differential-algebraic equations

$$\dot{x} = f(x, y, P_{ref}) \tag{11}$$

$$0 = g(x, y, P_{ref}) \tag{12}$$

with the state vector $x = [\delta \quad \omega]^T \in \mathbb{R}^{2(n_g-1)}$, the vector of algebraic variables $y = [i_x \quad i_y \quad V \quad \theta]^T \in \mathbb{R}^{2(n_b+n_g-1)}$. f is composed of the differential equations (1) and (2) to represent each $(2n_g - 1)$ generators, g is composed of the algebraic equations (5) and (6) for each $(2n_g - 1)$ generators, and $2n_b$ grid equations.

Note that the consideration of neglecting damping terms leads to an oscillatory behavior of the dynamical system when subject to a disturbance. Then, the switching operation can be pictured as shown in Fig. 2 [14], and described as follows: initially, the system is considered to be in steady-state at the equilibrium point x_e, but the state variables are shifted away from the equilibrium because of a disturbance, such as a short-circuit. At time t_0 the short-circuit is cleared and the states at that time are $x(t_0) = x_0$. As shown in Fig. 2-(a), after the short-circuit, the system will exhibit a periodic trajectory (black dashed line) centered at x_e. The DEOC is activated at some point along the trajectory when $x(t = t_{st}) = x_{st}$ (st: switching time), and the system will shift its trajectory to another periodic orbit centered at the controlled equilibrium point x_{ce}–described by the red dashed line in Fig 2.

In the optimal case, x_e belongs to the controlled orbit, then t_{off} is set to t when $x(t) = x_e$. The entire DEOC operation will lead the system through the blue trajectory, ultimately eliminating the oscillation. Fig. 2-(b) shows a case when the switch-on is performed slightly after $x(t) = x_{st}$. In this case, x_e would not belong to the controlled periodic trajectory and the oscillation cannot be annihilated. If the switching is not performed at the optimal time, a sub-optimal trajectory near the equilibrium point x_e will be desirable.

C. Power injection from controllable components

The objective of the DEOC operation is to significantly reduce the oscillations associated with the most excited modes of the system. Along these lines, one possible solution to tackle multi-mode systems is to progressively target one mode at a

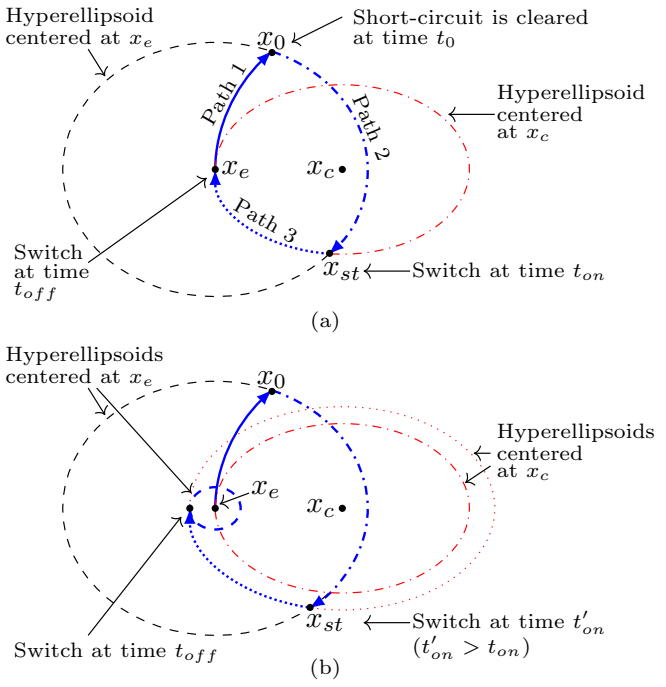

Fig. 2. Graphical description of system trajectories with DEOC [14]: (a) optimal solution, (b) sub-optimal solution.

time through the injection/absorption of active power from controllable components.

The linearization around the stable equilibrium point $z_e = [x_e \quad y_e \quad P^0_{ref}]^T$ is given by

$$\Delta\dot{x} = \left.\frac{\partial f}{\partial x}\right|_{z_e} \Delta x + \left.\frac{\partial f}{\partial y}\right|_{z_e} \Delta y = J_1\Delta x + J_2\Delta y \tag{13}$$

$$0 = \left.\frac{\partial g}{\partial x}\right|_{z_e} \Delta x + \left.\frac{\partial g}{\partial y}\right|_{z_e} \Delta y = J_3\Delta x + J_4\Delta y \tag{14}$$

Note that in steady state the power injection from CCs $\Delta P = 0$. Then, applying Kron's reduction to eliminate algebraic variables leads to

$$\Delta\dot{x} = \underbrace{\left[J_1 - J_2 J_4^{-1} J_3\right]}_{A_{sys}} \Delta x \tag{15}$$

From the system matrix, A_{sys} right-eigenvectors v_i and corresponding eigenvalues λ_i can be computed such that $A_{sys}v_i = \lambda_i v_i$ for all $i = 1, 2, \ldots, n$ with n being the number of states. In a matrix form: $V = [v_1 \quad v_2 \quad \cdots \quad v_n]^T$, and $\Lambda = \text{diag}\{\lambda_1, \lambda_2, \cdots, \lambda_n\}$. Consider the oscillation of the k-th mode is targeted for elimination. For that particular mode, one can define the projection $P = MM^T \in \mathbb{R}^{n\times n}$ with $M \in \mathbb{R}^{n\times 2}$ being the output matrix from the orthogonalization of $\bar{M} = [q_1 \quad q_2]$ over the range($\bar{M}$) using the Gram-Schmidt process [16]. Here, $q_1 = \text{Re}(v_k)$ and $q_2 = \text{Im}(v_k)$ are the basis of the 2-dimensional projected space, with v_k being the k-th eigenvector corresponding to the eigenvalue λ_k. The projection of a vector $\Delta x \in \mathbb{R}^n$ over range(M) is given by $P\Delta x$. In a similar fashion, an orthogonal subspace to range(M) is defined as: $N = \text{Null}(M) = \{a \in N \mid Ma = 0\}$, $N \in \mathbb{R}^{n\times(n-2)}$. The projector over the null space of M is given by $P_n = NN^T$. The projected vector is $P_n\Delta x$.

Now, the representation of the projected vector onto the range(M) and range(N) is determined as:

$$\alpha = \overbrace{(M^TM)^{-1}M^T \underbrace{MM^T}_{P}}^{S} \Delta x = M^T\Delta x \tag{16}$$

$$\alpha_n = \overbrace{(N^TN)^{-1}N^T \underbrace{NN^T}_{P_n}}^{S_n} \Delta x = N^T\Delta x \tag{17}$$

respectively. The orthogonal projector matrices P and P_n are very useful to target one mode at a time without exciting others due to the shifting of the equilibrium point. To annihilate the oscillation of the dominant mode, the DEOD will affect the equilibrium point over the range(M) and there will be no displacement over the range(N). This means that the projected orbits related to any mode but the targeted k-th mode will have no shifting in the equilibrium point due to the DEOC [15].

Note that the linear transformations S and S_n can be decomposed into two block matrices $S = [S_1 \quad S_2]$ and $S_n = [S_{n1} \quad S_{n2}]$ with proper dimensions, since $\Delta x = [\Delta\delta \quad \Delta\omega]^T$.

Following (16) and (17), the projected displacement of the equilibrium point onto range(M) and its orthogonal subspace are given by $\Delta\alpha = S_1\Delta\delta_e$ and $\Delta\alpha_n = S_{n1}\Delta\delta_e$, respectively. with $\Delta\delta_e = \delta_c - \delta_e$. A sufficient condition to have zero displacement onto the null(M) is: $\alpha_n = 0 = S_{n1}\Delta\delta_e$. By solving for $\Delta\delta_e$, the required controlled equilibrium point x_c is defined. This solution is given by:

$$\Delta\delta_e = K\bar{d} \in \text{Null}(S_{n1}) : |\bar{d}| = 1 \tag{18}$$

where K is a constant real parameter, and $\bar{d}$ is the unit direction vector of displacement of the equilibrium point to ensure $\alpha_n = 0$.

Now, to translate these results in terms of power injection/absorption ΔP by EIRs, consider the following linear model that includes the effect of CCs at non-generator buses

$$\Delta\dot{x} = J_1\Delta x + J_2\Delta y \tag{19}$$

$$0 = J_3\Delta x + J_4\Delta y + J_5\Delta P \tag{20}$$

with the sensitivity matrix $J_5 = \partial g/\partial P_{ref}|_{z_e}$. Using Kron's reduction to eliminate algebraic variables, and considering that in steady-state $\Delta\dot{x} = 0$, we get a relationship between the static displacement of the equilibrium point $\Delta x_e = [\Delta\delta_e \quad 0]^T$ with the power injection/absorption ΔP by CCs

$$\Delta P = [J_2J_4^{-1}J_5]^+[J_1 - J_2J_4^{-1}J_3]\Delta\delta_e \tag{21}$$

where the operator $^+$ denotes the pseudo-inverse. With this specific ΔP, the equilibrium point is only displaced on the representation over the projected subspace range(M). However, this formulation requires power injection/absorption at all non-generator buses, which is non-realistic for a practical application where we only count for just a few CCs.

In order to reduce the number of required controllers for DEOC operation, the mode controllability [17] can be used, defined as

$$CONT_{kj} = |w_k^T B_j| \tag{22}$$

where w_k is the k-th left eigenvector of the system matrix A_{sys} and B_j denotes the j-column vector of the input matrix B. This index exhibits the controllability of mode k from the j-bus. The mode controllability is used to determine a controller combination in the sense of minimizing the control action ΔP required. This index can be determined from the linear model of equations (19) and (20) considering the input as ΔP and corresponding input matrix $B = -[J_2 J_4^{-1} J_5]$, which in this context expresses the sensitivity of the displacement equilibrium point onto the targeted k-th mode with respect to the power injection/absorption at the j bus.

This index is effective in reducing the number of buses where control action ΔP is required. After the subset of CCs is defined, by the least square problem associated with the pseudo-inverse, we achieve a minimum displacement of the equilibrium point onto the null(M) by defining the injection/absorption by CCs as

$$\Delta P^* = A \Delta P \tag{23}$$

where A is a diagonal matrix composed of zeros and ones according to the buses where CCs are deployed. Note that once the oscillation of the targeted dominant mode has been annihilated through DEOC, the process can be repeated to shift the equilibrium point on the representation over the projected subspace range(M)–now related to the second dominant mode and so on.

D. Switching conditions

As mentioned before, in order to perform a successful DEOC operation the activation time t_{on} should be obtained such that the controlled dynamic evolution (red dashed hyper-ellipsoid centered at x_c in Fig. 2) contains the system equilibrium point x_e. In the same way, when the dynamic evolution is close to the equilibrium, the goal is to restrain oscillations after DEOC is turned off, leading to a significant reduction in the oscillation but not complete annihilation. As developed in [14] and [15], a switching function to determine the switch-on time and energy-based switch-off rule are considered.

1) Switch-on time: based on the linear model around the pre-fault steady-state equilibrium point the following switching function:

$$\begin{aligned} h(x) &= 2(x_e - x_c)^T D (x_e - x_c) \\ &\quad - (x - x_c)^T (D + A_{sys}^T E A_{sys})(x - x_c) \in \mathbb{R} \end{aligned} \tag{24}$$

can effectively determine the switching time when $h(x) = 0$. Where $D = (V^{-1})^* V^{-1}$, $E = (V^{-1})^* (\Lambda^{-1})^* \Lambda^{-1} V^{-1}$, and the operator * denotes the conjugate transpose. Note that D and E are real positive definite matrices.

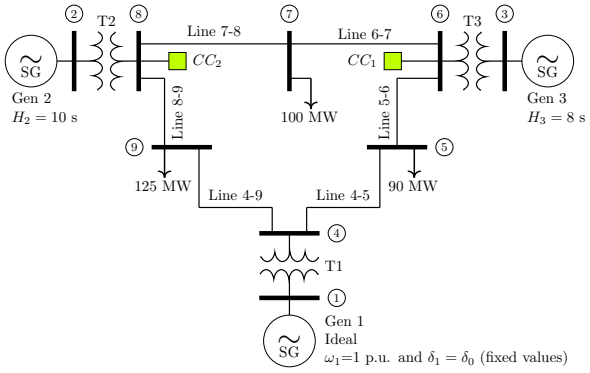

Fig. 3. 9-bus system with added controllable components.

2) Switch-off time: An energy-based approach can be used to ensure that the switch back to the equilibrium point x_e is done appropriately. The oscillation energy is defined as the summation of the individual kinetic energy of the SGs [18]

$$E_k(t) = \sum_{j=1}^{n_g} H_j \omega_s \Delta\omega_j^2 \tag{25}$$

where $\Delta\omega_j$ is the speed deviation of SG j in per unit, and H_j is the inertia constant of SG j in seconds. When $E_k(t)$ is reduced, the oscillation will be shrunk and the states will be confined to a closer orbit around the equilibrium point hence considerably reducing oscillation amplitude. Thus, when the states x are orbiting around the controlled equilibrium x_c as DEOC is on, set $t_{off} = t$ if at a particular time t, $E_k(t)$ reaches a minimum. Note that also a proximity function in terms of the norm between the states and the equilibrium point projections into the targeted subspace can also be used to determine the switch-off time.

If performed at the optimal time, the switch-off is done exactly at the original equilibrium point, thus completely annihilating the targeted oscillation. Otherwise, a sub-optimal operation that significantly reduces the oscillation is sought.

III. Simulation Results and Analysis

Simulations are performed in a modified 9-bus system shown in Fig. 3. Grid parameters are obtained from the MATPOWER library [19]. This system exhibits two electromechanical modes of oscillation: one inter-area oscillation between G1 (slack bus) and G2-G3, and another local oscillation between G2 and G3. No additional controllers are contemplated to evaluate the sole action of the proposed DEOC. EIRs are generically considered controllable components and are located within the grid based on energy potential or technical considerations. In this case, the mode controllability is used to determine CC location. Based on this index, two controllable components are considered to be deployed at buses 6 and 8 which are the two buses with the highest controllability for both oscillatory modes of the system as shown in Table I. Additionally, for the sake of simplicity, both CCs are set to have $P_{ref}^0 = 0$.

TABLE I
9-BUS SYSTEM MODE CONTROLLABILITY

Bus i	$CONT_{1i}$	$CONT_{2i}$
4	0.302	0.001
5	0.537	0.113
6	0.972	0.323
7	0.966	0.043
8	0.961	0.304
9	0.530	0.105

Two highly loaded scenarios are taken into consideration for analysis and performance of the DEOC operation. Each scenario is set to increase the active power flow related to each mode of oscillation near the static stability limit. They are defined as:

- Scenario 1: Increase load at bus 9 in 400% and generation of SG3 proportionally, which mainly increases the real power flow in the path from SG3 to bus 4.
- Scenario 2: Increase load at bus 7 in 400% and generation of SG2 and SG3 proportionally, which makes the real power flow related to the local mode to become greater.

A. Scenario 1

Simulations are carried out considering a self-cleared three-phase fault applied at bus 5 at $t = 1$ s with a total duration of 5 cycles. Under this scenario, the local and inter-area mode frequencies are 1.74 Hz and 0.78 Hz, respectively. Then, to handle both modes, two discrete actions are required from CCs, starting with the 0.78 Hz mode which is the most excited mode due to the disturbance.

Results comparison between the base case (no control) with the DEOC operation is summarized in Fig. 4. For the sake of simplicity, only state variables δ and ω are shown. First, it is appreciable that the uncontrolled dynamic response is a combination of the two modes of oscillation, which is induced by the high load condition of the grid and the location of the disturbance (compare with results from [15]). Second, the discrete control applied validates the performance of the DEOC with a highly noticeable reduction of the oscillation amplitude in the dynamic response. Note that in a practical operation scenario, where damping is considered, SG dampers and PSSs would take care of the remaining oscillation.

By using the switching function $h(x)$ to determine the switch-on time and local minimum oscillation energy $E_k(t)$ to define the switch-off time on each controllable component, resulting in the following discrete operation:

$$CC_1 : \Delta P_6 = \begin{cases} -22.71 \text{ MW} & \text{if } 1.566 \text{ s} < t < 2.046 \text{ s} \\ -63.27 \text{ MW} & \text{if } 2.408 \text{ s} < t < 2.633 \text{ s} \\ 0 & \text{otherwise} \end{cases}$$

$$CC_2 : \Delta P_8 = \begin{cases} -34.60 \text{ MW} & \text{if } 1.566 \text{ s} < t < 2.046 \text{ s} \\ 59.38 \text{ MW} & \text{if } 2.408 \text{ s} < t < 2.633 \text{ s} \\ 0 & \text{otherwise} \end{cases}$$

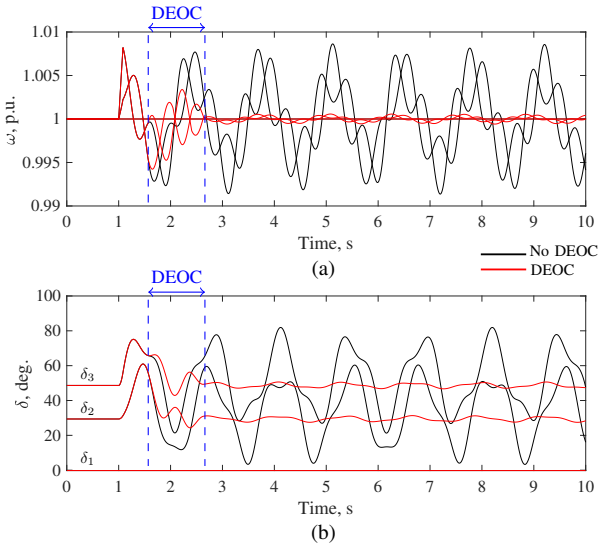

Fig. 4. 9-bus system dynamics comparison, scenario 1: (a) SG speeds, (b) torque angle.

B. Scenario 2

In this case, a self-cleared three-phase fault was applied at bus 6 at $t = 1$ s with a total duration of 5 cycles. Due to the loadability of the system, the local and inter-area mode frequencies are slightly different than scenario 1, in this case being 1.80 Hz and 0.93 Hz, respectively. Similarly, two discrete actions are required from CCs to reduce the amplitude of the oscillation of the overall response.

Simulation results are shown in Fig. 5. Once again the effectiveness of the DEOC is exhibited in the controlled dynamics. However, just like in scenario 1, only a sub-optimal solution is achieved. This is due to intrinsic deviations of the linear model –used to define the switching function $h(x)$– with respect to the actual nonlinear model of the system. However, as expected, the sub-optimal switching leads to an oscillation amplitude confined around the equilibrium point.

The operation of each controllable component is summarized as follows:

$$CC_1 : \Delta P_6 = \begin{cases} -4.20 \text{ MW} & \text{if } 1.442 \text{ s} < t < 1.828 \text{ s} \\ -41.65 \text{ MW} & \text{if } 2.335 \text{ s} < t < 2.565 \text{ s} \\ 0 & \text{otherwise} \end{cases}$$

$$CC_2 : \Delta P_8 = \begin{cases} 6.81 \text{ MW} & \text{if } 1.442 \text{ s} < t < 1.828 \text{ s} \\ 38.16 \text{ MW} & \text{if } 2.335 \text{ s} < t < 2.565 \text{ s} \\ 0 & \text{otherwise} \end{cases}$$

IV. CONCLUSION

In this paper, the performance of the discrete control for oscillations when considering more realistic control and load scenarios is studied. The main novel features in this work with respect to previous efforts on the DEOC problem are the inclusion of a nonlinear model for the grid and the reduction of required controllable components for discrete control actions.

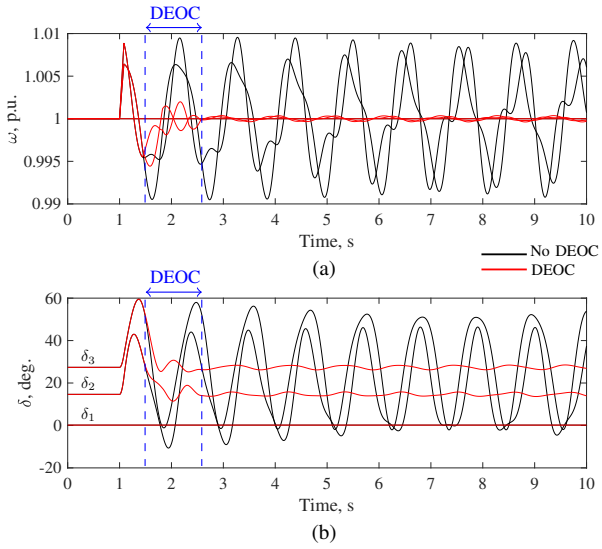

Fig. 5. 9-bus system dynamics comparison, scenario 2: (a) SG speeds, (b) torque angle.

Both upgrades have been shown to only account for a small deviation from the optimal solution proposed for a fully linear model. The effectiveness of the DEOC operation is demonstrated by means of simulations of the 9-bus system for two highly loaded scenarios. Even though an optimal solution is not achieved, in both cases the sub-optimal solution significantly reduces the oscillation amplitude to be confined in a small region around the equilibrium point. Future work will take into consideration the inclusion of detailed models for generators, e.g., the two-axis model, and its corresponding controllers into the DEOC performance.

REFERENCES

[1] B. Kroposki, "Integrating high level of variable renewable energy into electric power systems (NREL-PR-5D00-68349)," Power Systems Engineering Center, National Renewable Energy Lab., Tech. Rep., 2018.

[2] J. Slootweg and W. Kling, "The impact of large scale wind power generation on power system oscillations," *Electric power systems research*, vol. 67, no. 1, pp. 9–20, 2003.

[3] J. Slootweg, S. De Haan, H. Polinder, and W. Kling, "Simulation of electrical power systems with a high wind energy penetration," in *36th IEA R&D Wind Topical Expert Meeting: Large Scale Integration into the Grid, Newcastle*, 2001, pp. 113–126.

[4] Y. Wang, H. Silva-Saravia, and H. Pulgar-Painemal, "Actuator placement for enhanced grid dynamic performance: A machine learning approach," *IEEE Transactions on Power Systems*, vol. 34, no. 4, pp. 3119–3128, 2019.

[5] H. Pulgar-Painemal, Y. Wang, and H. Silva-Saravia, "On inertia distribution, inter-area oscillations and location of electronically-interfaced resources," *IEEE Transactions on Power Systems*, vol. 33, no. 1, pp. 995–1003, 2017.

[6] R. Muhamad, *Stability analysis of transmission systems with high penetration of distributed generation*, 2006.

[7] D. Cai, P. Wall, M. Osborne, and V. Terzija, "Roadmap for the deployment of wampac in the future gb power system," *IET Generation, Transmission & Distribution*, vol. 10, no. 7, pp. 1553–1562, 2016.

[8] H. Zhang, "Peak Reliability synchrophasor technology roadmap for control room solution," Peak Reliability, EMS Network Apps. Manager. RC User Group Meeting, Denver, CO, USA, Tech. Rep., 2017.

[9] N. Ratmarao and D. K. Reitan, "Improvement of power system transient stability using optimal control: Bang-bang control of reactance," *IEEE Transactions on Power Apparatus and Systems*, vol. PAS-89, no. 5, pp. 975–984, 1970.

[10] D. Kosterev and W. Kolodziej, "Bang-bang series capacitor transient stability control," *IEEE Transactions on Power Systems*, vol. 10, no. 2, pp. 915–924, 1995.

[11] J. Chang and J. Chow, "Time-optimal series capacitor control for damping interarea modes in interconnected power systems," *IEEE Transactions on Power Systems*, vol. 12, no. 1, pp. 215–221, 1997.

[12] D. K. Reitan and N. RamaRao, "A method of improving transient stability by bang-bang control of tie-line reactance," *IEEE Trans. on Power Apparatus and Systems*, vol. PAS-93, no. 1, pp. 303–311, 1974.

[13] N. P. Johansson, H.-P. Nee, and L. Angquist, "Discrete open loop control for power oscillation damping utilizing variable series reactance facts devices," in *Proceedings of the 41st International Universities Power Engineering Conference*, vol. 2. IEEE, 2006, pp. 785–789.

[14] H. Pulgar-Painemal and S. Martinez-Lizana, "On the search for expanded grid control capabilities: Discrete control on emerging power technologies," *arXiv:2209.06239 [eess.SY]*, 2022.

[15] S. Martinez-Lizana and H. Pulgar-Painemal, "Further advances on discrete electromechanical oscillation control," in *2022 North American Power Symposium (NAPS)*, 2022, pp. 1–6.

[16] L. N. Trefethen and D. Bau, *Numerical linear algebra*. Siam, 2022, vol. 181.

[17] M. Aboul-Ela, A. Sallam, J. McCalley, and A. Fouad, "Damping controller design for power system oscillations using global signals," *IEEE Transactions on Power Systems*, vol. 11, no. 2, pp. 767–773, 1996.

[18] H. Silva-Saravia, H. Pulgar-Painemal, D. A. Schoenwald, and W. Ju, "Adaptive coordination of damping controllers for enhanced power system stability," *IEEE Open Access Journal of Power and Energy*, vol. 7, pp. 265–275, 2020.

[19] R. D. Zimmerman, C. E. Murillo-Sánchez, and R. J. Thomas, "Matpower: Steady-state operations, planning, and analysis tools for power systems research and education," *IEEE Transactions on Power Systems*, vol. 26, no. 1, pp. 12–19, 2011.